Proceedings of ASME Turbo Expo 2019
Turbomachinery Technical Conference and Exposition
GT2019
June 17-21, 2019, Phoenix, Arizona, USA

GT2019-90980

DESIGN OF HIGH SPECIFIC SPEED MIXED FLOW MICRO-COMPRESSOR FOR CO-FLOW JET ACTUATORS

Kewei Xu*
Gecheng Zha†
Department of Mechanical and Aerospace Engineering
University of Miami
Coral Gables, Florida 33124
Emails: kxx50@miami.edu , gzha@miami.edu

ABSTRACT

This paper conducts aerodynamic design of a high specific speed mixed flow micro-compressor used as an actuator for Co-flow Jet (CFJ) Active Flow Control (AFC) airfoil. The aerodynamic design poses several challenges, including: 1) Small size with very low Reynolds number; 2) High specific speed for mixed-flow compressor due to high mass flow rate and low total pressure ratio; 3) Static pressure ratio lower than 1 to match the low pressure of CFJ airfoil leading edge (LE) suction peak.

The numerical design approach is validated with a mixed flow micro-compressor with very good agreement between the predicted performance and the measured data. Front loaded rotor blade work distribution is adopted to decrease boundary layer loss at the blade surface. Free vortex work distribution is applied for the rotor span to reduce spanwise mixing loss. The rotor efficiency achieved by the numerical prediction is 91.7%. Significant loss is observed downstream of the rotor when the flow reaches the stator and the outlet guide vane (OGV). For the stator, it is found that an inlet and outlet flow path area ratio of 1.05 achieves a very high total pressure recovery of 99.29%. A very good stage isentropic efficiency of 84.3% is achieved. The final design of micro-compressor achieves a flow coefficient of 0.3 at the design point with a total pressure ratio of 1.117 and a static pressure ratio of 0.987. A structure FEM analysis indicates that the rotor blades satisfy the structure strength and modal frequency requirement.

NOMENCLATURE

Latin alphabet

D	Diameter (mm)
D_f	Diffusion Factor (-)
D_s	Specific Diameter, $D_{2t}\frac{(\Delta h_s)^{0.25}}{(\dot{Q})^{0.5}}$ (-)
$\dot{Q}$	Volume Flow rate (m^3/s)
$\dot{m}$	mass Flow rate (kg/s)
m_{cor}	Corrected Mass Flow Rate, $\dot{m}\frac{\sqrt{T_0}}{p_0}$ (-)
Δh_s	Isentropic Total Enthalpy Rise, $C_pT_{01}[(\pi_{t-t})^{\frac{\gamma-1}{\gamma}}-1]$ (J/kg)
Δh_{Euler}	Actual Total Enthalpy Rise (Euler Work), $C_pT_{01}(\tau_{t-t}-1)$ (J/kg)
R_{mo}	Radius of Motor (mm)
R_h	Radius of Compressor Hub (mm)
U	Circumferential Speed (m/s)
W	Relative Velocity (m/s)
Z	Blade Number (-)

Greek alphabet

ω	Angular Velocity (radians/s)
ω_s	Specific Speed, $\omega\frac{(\dot{Q})^{0.5}}{(\Delta h_s)^{0.75}}$ (-)

*Ph.D. Candidate
†Professor, ASME Fellow

Copyright © 2019 by ASME

ϕ	Flow Coefficient, $\frac{\dot{Q}_1}{D_{2t}^2 U_{2t}}$ (-)
π_{s-t}	Static to Total Pressure Ratio (-)
π_{t-t}	Total to Total Pressure Ratio (-)
τ_{t-t}	Total to Total Temperature Ratio (-)

Abbreviation

CFJ	Co-flow Jet
AFC	Active Flow Control
TE	Trailing edge
LE	Leading edge
RPM	Round per Minute
OGV	Outlet Guide Vane
SM	Surge Margin

Subscript

0	Total
1	Impeller Inlet
2	Impeller Outlet
t	Tip
s	Isentropic, Specific
s-t	Static to Total
t-t	Total to Total

INTRODUCTION

Mixed flow compressors are able to achieve both high mass flow rate and high pressure rise, which combines the merits of axial and centrifugal compressor. Recently, increasing attention is paid to mixed compressor design driven by the interest of more and more micro-compressor applications, in particular in the field of active flow control.

Musgrave and Plehn [1] designed a single stage mixed flow compressor with a pressure ratio of 3.02 and the rotor efficiency of 0.91. Monig et al [2, 3] studied the mixed flow impeller with a pressure ratio of 5. Their experimental results suggested that a high outlet Mach number is unfavorable for downstream diffuser. A high-specific speed (ω_s) centrifugal compressor with ω_s of 1.8 was designed by Rodgers [4]. It sets the benchmark that represents the performance potential of high ω_s centrifugal compressor. Casey et al [5] developed a new equation for Cordier line in the mixed flow region, which provides a guideline for the preliminary design of mixed flow compressors. They then designed a transonic mixed flow compressor stage with a very high flow coefficient of 0.25 and an isentropic pressure rise coefficient of 0.56 [6]. The effects of Reynolds number on centrifugal and mixed-flow compressor are also studied [7–10]. Previous studies are more focused on the design of mixed flow compressor with high loading, but not much attention is paid to the design of mixed flow compressors with low enthalpy rise, high mass flow rate and high specific speed, which has great application potential as actuators for Co-flow Jet (CFJ) active flow control (AFC).

Among various AFC techniques, Co-flow Jet is a zero-net mass-flux (ZNMF) flow control method recently developed by Zha et al. [11–23]. It is demonstrated numerically and experimentally that CFJ achieves significant improvements on airfoil lift augmentation, drag reduction and stall margin enlargement.

In a CFJ airfoil, electric micro-compressors along with suction and injection ducts are embedded inside the airfoil as shown in Fig.1. The micro-compressor works as an actuator that draws flow near trailing edge (TE), pressurizes the flow and ejects it as a jet near leading edge (LE).

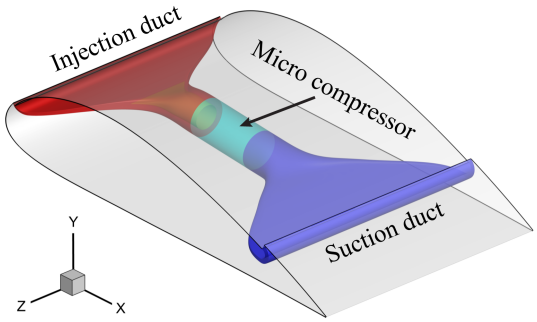

FIGURE 1: Schematics of the CFJ airfoil with embedded micro-compressor

Such application of CFJ actuators poses challenging requirements for the micro-compressor design: 1) Small size with very low Reynolds number. For example, the micro-compressor used in the recent CFJ airfoil wind tunnel experiment [24] has a diameter less than 8 cm and the Reynolds number based on the impeller diameter is 55,000. The low Reynolds number makes the flow prone to separation and the viscous loss needs to be handled with particular attention. 2) Very high specific speed for a mixed-flow compressor due to the required high mass flow rate and low enthalpy rise for flow control. These two factors push ω_s to the high end of mixed compressor region in Cordier line, where a high efficiency design is challenging. 3) The required static pressure ratio (π_{s-t}) lower than 1 to match the low pressure of CFJ airfoil leading edge suction peak. Total pressure and static pressure are typically increased simultaneously through compressor. However, CFJ actuator is required to increase the total pressure to compensate the loss and decrease the static pressure to match the airfoil leading edge suction pressure. Therefore, a high efficiency outlet guide vane with a nozzle is required at compressor outlet to decrease the outlet static pressure.

This paper describes the design approach for a high specific speed mixed flow micro-compressor as a CFJ actuator. The im-

Copyright © 2019 by ASME

peller blade loading is optimized with minimum loss. Different chordwise and spanwise work distributions are studied to maximize the stage efficiency.

DESIGN REQUIREMENTS

The design requirements are to maximize the mass flow rate with a total pressure of 1.13 at the design RPM of 93,000. The design has geometry constraints of maximum casing diameter of 75 mm, maximum length of 135 mm, specific speed of 3.3, efficiency greater than 80% and RPM varying from the design RPM by $\pm$30%. The designed flow coefficient is about 0.3, which is the result of the high mass flow rate requirement within a small size flow path. The maximum power is determined by the volume inside the compressor hub that can fit a motor. The compressor hub radius (R_h) is required to be 3mm higher than motor radius (R_{mo}).

DESIGN METHOD

The preliminary design and geometrical selection of compressor impeller are based on the Cordier diagram in literature [5, 25, 26] as shown in Fig. 2 and 3, which describe the relationship between specific speed (ω_s) and specific diameter (D_s) for the optimum compressor efficiency.

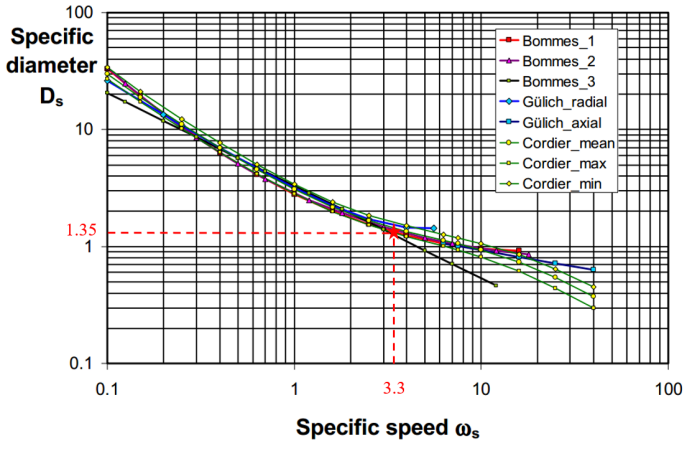

FIGURE 2: Various equation systems for the Cordier line (adopted from [5])

The ω_s and D_s in Fig. 2 and 3 are the specific speed and specific diameter defined below:

$$\omega_s = \omega \frac{(\dot{Q})^{0.5}}{(\Delta h_s)^{0.75}} \tag{1}$$

$$D_s = D_{2t} \frac{(\Delta h_s)^{0.25}}{(\dot{Q})^{0.5}} \tag{2}$$

where ω is the rotor angular velocity, $\dot{Q}$ is the volume flow rate, Δh_s is the rotor isentropic total enthalpy change, and D_2t is the impeller outlet casing diameter.

According to the Cordier lines, to achieve high compressor efficiency, axial compressors in general have high specific speeds and low specific diameters, while centrifugal compressors have low specific speeds and high specific diameters [5, 27]. For the present design, the specific speed is 3.3 and the specific diameter is 1.35, which roughly falls outside of the upper boundary of mixed compressors range on the Cordier line marked as the red star in Fig. 2.

Specific speed is also used to select the type of compressor to be used. As shown in Fig. 3, different specific speed range corresponds to different machine types. Typically, a centrifugal compressor will have $\omega_s < 0.5$, a mixed flow compressor has $0.5 < \omega_s < 1.5$, and an axial compressor has $\omega_s > 2$ [5]. The present design has the specific speed at high end of mixed flow compressor, where high efficiency design is hard to achieve. An axial compressor is supposed to be the option. However, in order to have sufficient volume to embed the electric motor inside the hub of the compressor, a mixed compressor configuration is desirable. A mixed flow compressor has a gradually increasing hub radius, which has more space to fit an electric motor. Relatively speaking, an axial compressor has little radius increment at hub and therefore the motor needs more axial space to fit, which increases the overall length of the compressor. One may argue that an axial compressor could have a higher hub radius at rotor inlet so that a motor can be fitted underneath the compressor hub. However, this is not feasible for the present design requirement. Because a high hub radius increases blade work at the same rpm, the total pressure rise will be significantly higher than targeted total pressure ratio (π_{t-t}=1.13). Overall, a mixed flow configuration is best option for its compactness and low total pressure ratio requirement.

Copyright © 2019 by ASME

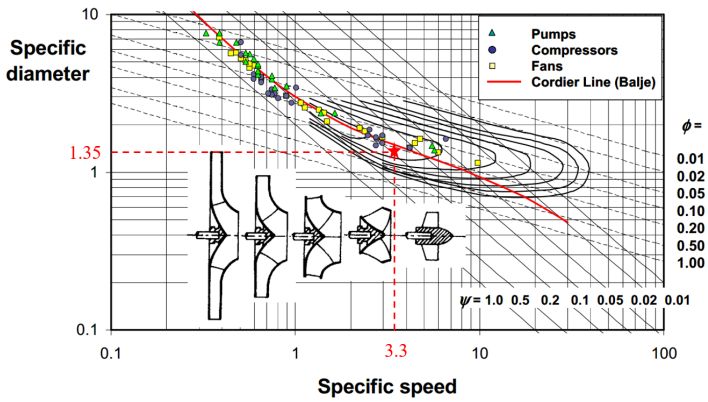

FIGURE 3: Cordier diagram with different turbomachines (picture adopted from [5])

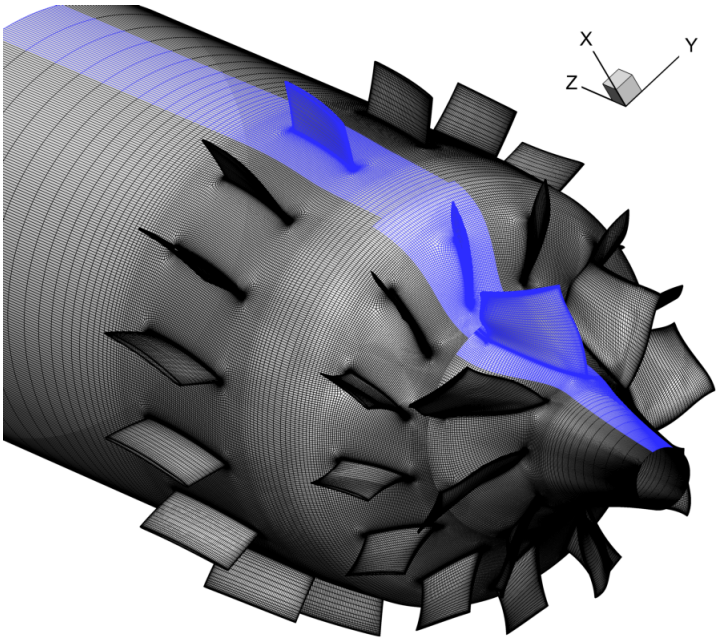

FIGURE 4: Computational mesh of the present micro-compressor simulation

The meridional plane blade profiles are designed using an in house S2 plane throughflow code. The code distributes the targeted work in span and calculates the blade turning based on the work distribution.

The 3D design is conducted using steady state CFD simulation using ANASYS CFX code. The computational domain has single blade passage with multi-blade rows, which consists of a converging intake, an impeller passage, a stator passage and a OGV passage with a downstream nozzle. Fig. 4 (in blue) shows the structured mesh with a size of 720000 nodes generated by Turbogrid. The rotor mesh has 50 points spanwise, 9 points in the tip clearance and 170 points around the blade. The mesh refinement study indicates that the results are converged based on the mesh size. Turbulent effects are simulated by the k-ω shear stress transport (SST) turbulent model to better capture the flow separation. The mixing interface boundary conditions are applied on the interfaces between blade rows. The convergence criterion is that the residual reduced by 4 orders of magnitude.

DESIGN APPROACH VALIDATION

A micro-compressor with the similar size and Reynolds number designed by PCA [28], manufactured and tested by Celeroton [29] is used to validate the design tool and approach. The validated micro-compressor is also a mixed-compressor with a similar configuration as shown in Fig. 5, including impeller, stator, OGV and outlet duct. Besides, a casing treatment is also included in the design to extend the operating range [30]. The PCA micro-compressor has substantially lower mass flow rate and power. Its design point has total pressure ratio of 1.21, isentropic efficiency of 80.2%, specific speed of 1.48 and specific diameter of 2.55. The computed speedlines with the pressure ratio and efficiency are in excellent agreement with the measurement [29] as shown in Fig. 6, which has the mass flow rate normalized by the design point mass flow rate.

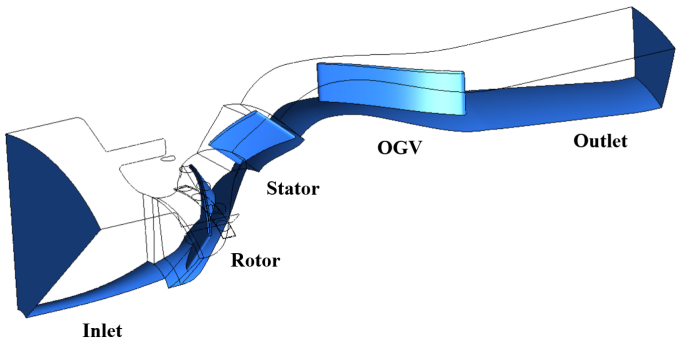

FIGURE 5: The configuration of the validated micro-compressor

Copyright © 2019 by ASME

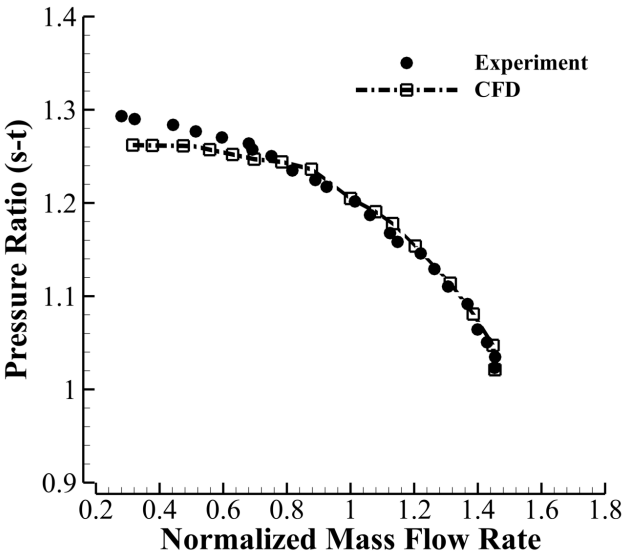

(a) Pressure ratio

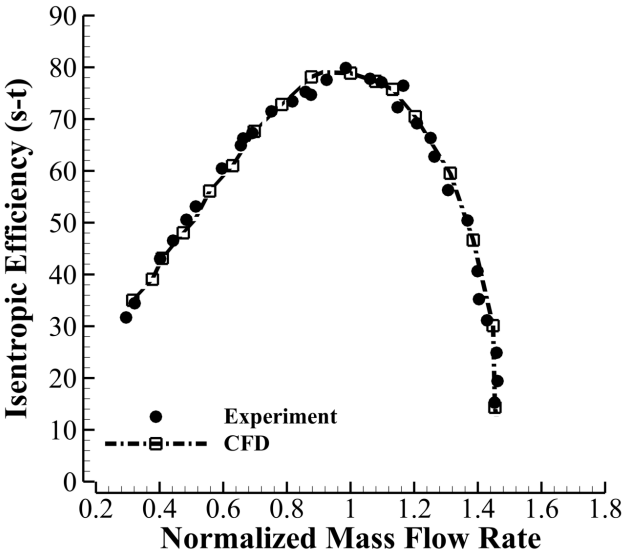

(b) Isentropic efficiency

FIGURE 6: Computed speedlines of a micro-compressor compared with the measured results [29]

The maximum discrepancy between the computed and measured pressure ratio and isentropic efficiency near stall are 2.32% and 2.1% respectively. The discrepancy is mostly due to the flow separation and complex vortical flow at near stall condition, for which the RANS turbulence model is unable to resolve.

MICRO-COMPRESSOR DESIGN

The main geometrical parameters of the present micro-compressor stage is presented in Table 1. The casing treatment is not included in the present design, but will be studied as the future work.

TABLE 1: Stage Geometrical Parameters

Rotor inlet hub diameter	18.1mm
Rotor inlet casing diameter	44.8mm
Rotor exit hub diameter	29.8mm
Rotor exit casing diameter	46.5mm
Tip clearance	0.16mm
Number of impeller blades	8
Stator inlet hub diameter	32.1mm
Stator inlet casing diameter	48.3mm
Stator exit hub diameter	58.3mm
Stator exit casing diameter	70.2mm
Number of Stator blades	13

Rotor Design

The micro-compressor stage consists of a mixed flow impeller and a stator. There is a balance between maximizing the mass flow rate and keeping a low total pressure ratio. To increase compressor mass flow rate, increasing RPM or enlarging flow path area can be considered. However, a high RPM and a large flow path area results in higher blade radius. Both lead to increased blade tangential velocity (U), which is limited by the blade material strength. The high tip tangential speed also tends to increase the total pressure to the level more than required. An effective approach used in this design is to open up impeller cascade throat area by decreasing the stagger angle as illustrated in Fig. 7. As the trailing edge B is moved downwards B', the cascade shape changes from the solid lines to the dashed lines. As the result, the blade stagger angle decreases from α to α' and the throat area is increased from T to T', which allows more mass flow to pass. The blade turning can be kept about the same as the stagger angle is decreased to maintain the same work amount.

For the present design, the stagger angle is decreased from 53° at tip to 28° at hub with blade turning angle adjusted to maintain the required rotor enthalpy rise. The required flow coefficient of 0.3 and total pressure ratio of 1.13 are satisfied. The final design for the impeller consists of eight blades with an forward sweeping of 30 degree to the radial direction at LE.

Copyright © 2019 by ASME

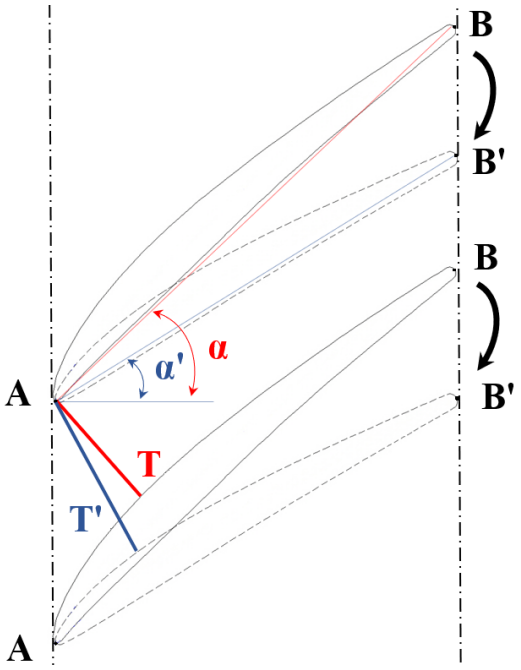

FIGURE 7: Illustration of the cascade open method

The design has a subsonic relative rotor tip Mach number of 0.76 as shown in Fig. 8. Fig. 9 shows the Mach number contours at different span. No shock wave is observed. Fig. 10 plots the normalized static pressure at blade surface of each span, for which the static pressure is normalized by inlet total pressure. Fig. 10 also shows that the blade is mostly front-loaded. Compared to other loading distribution, front loading minimizes the boundary layer thickening and opens up the throat area of blade channel. With such loading distribution, the impeller blade achieves a good isentropic efficiency of 91.7%.

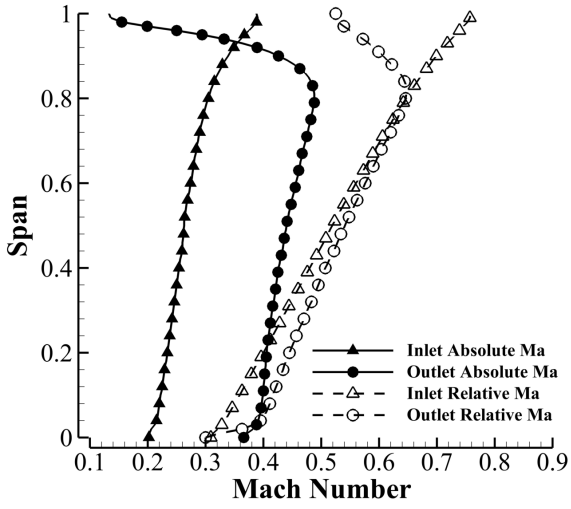

FIGURE 8: Mach number distribution at Rotor inlet and outlet

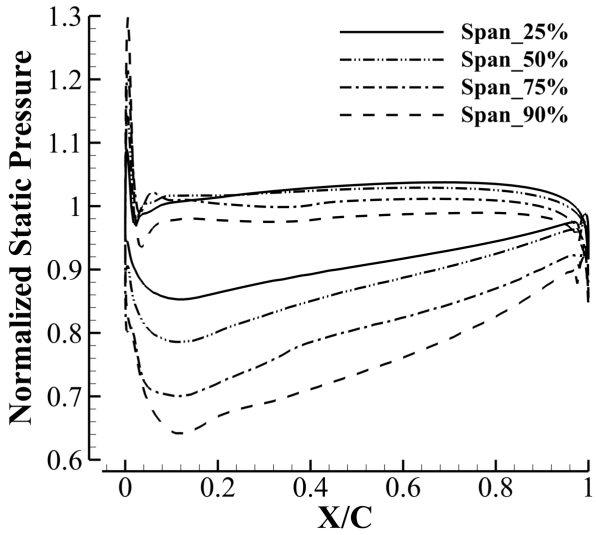

FIGURE 10: Spanwise normalized static pressure distribution of impeller blade

Diffusion factor (D_f) is another important parameter to indicate blade loading. The value of D_f suggests the diffusion extent that the flow experiences in a 2D compressor cascade. A modified diffusion factor is proposed by Coppage, J.E. [31] to compensate for the centrifugal effect in centrifugal compressors as defined below:

$$D_f = 1 - \frac{W_2}{W_{1t}} + \frac{0.75\Delta h_{Euler}/U_2^2}{(W_{1t}/W_2)[(Z/\pi)(1-D_{1t}/D_2)+2D_{1t}/D_2]} \quad (3)$$

Where, W_2 is the outlet relative velocity, W_{1t} is the inlet relative velocity at tip, Δh_{Euler} is the actual total enthalpy rise, U_2 is the outlet circumferential velocity, Z is the blade number, D_{1t} is inlet tip diameter and D_2 is the outlet diameter.

Fig. 11 shows the diffusion factor along the span for the present design. The D_f has the maximum at the hub and gradually decreases to the tip. This is because the blade passage experiences an increasing diffusion due to the rapid radius increase at the hub. Fig. 8 and 9 indicate that the flow condition is healthy with no flow separation at the hub even though the diffusion factor is high. It is attributed to the centrifugal force effect that energizes the flow. This is one advantage of the mixed compressor.

Copyright © 2019 by ASME

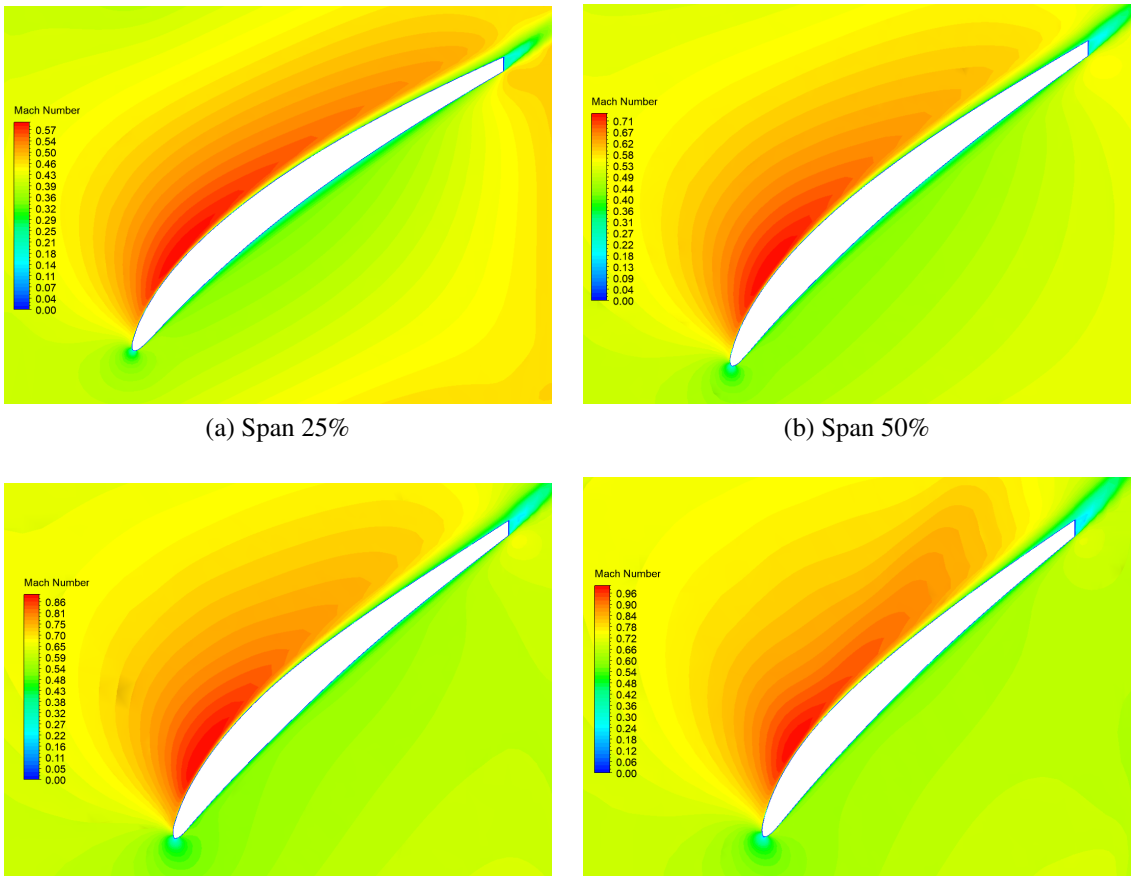

(a) Span 25%

(b) Span 50%

(c) Span 75%

(d) Span 90%

FIGURE 9: Spanwise Mach number contours

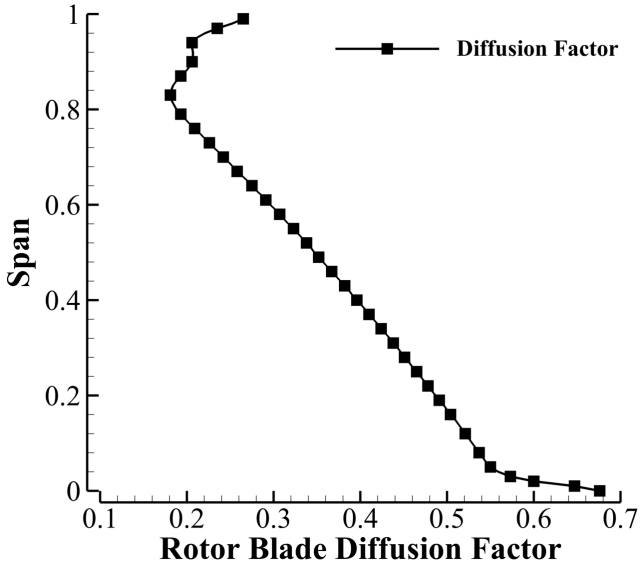

FIGURE 11: Diffusion factor of impeller blade

Three types of spanwise work distribution are studied as shown by the rotor outlet total pressure radial profile in Fig. 12: free vortex, hub strong, and tip strong. Free vortex has fairly equal work distribution along the span so that the spanwise mixing loss can be mitigated. Hub strong increases the hub work of impeller blade to release downstream stator blade loading at hub. Hub strong is usually applied on heavy duty stage to possess wider operating range. The present micro-compressor design is to achieve high mass flow rate and low total enthalpy rise. A hub strong design increases the downstream mixing loss. So is the tip strong work distribution. Fig. 13 shows the total pressure contours on the meridional plane of hub strong, tip strong and free vortex stage. The averaged total pressure is the same at the rotor outlet. All the geometry configurations downstream of the rotor are also the same. The contours show that the free vortex work distribution has more uniform total pressure downstream with less mixing loss, which results in the highest overall stage efficiency.

Copyright © 2019 by ASME

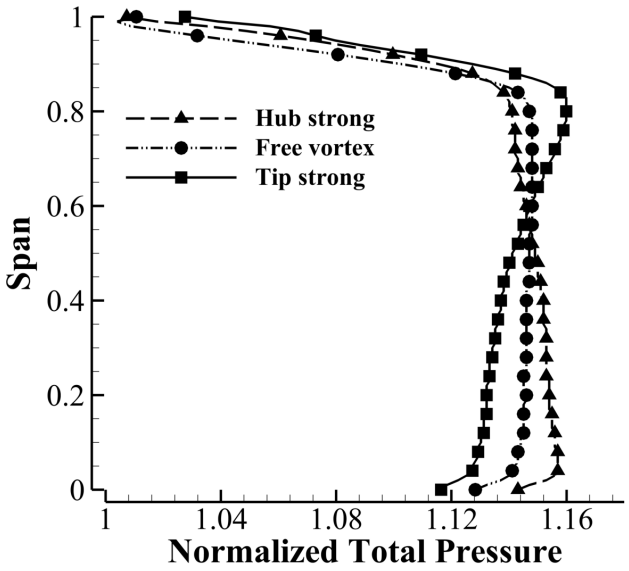

FIGURE 12: Work distribution

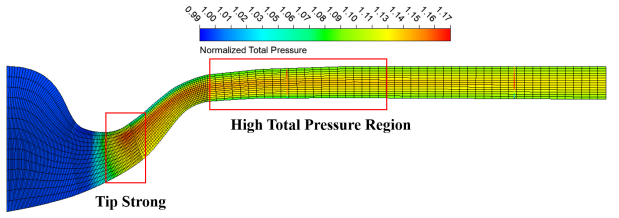

(a) Tip strong stage

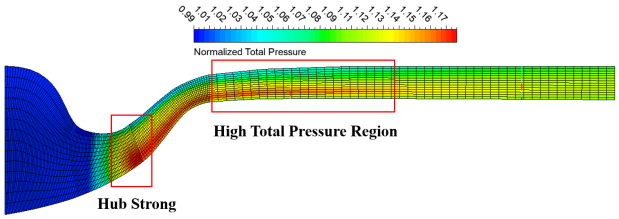

(b) Hub strong stage

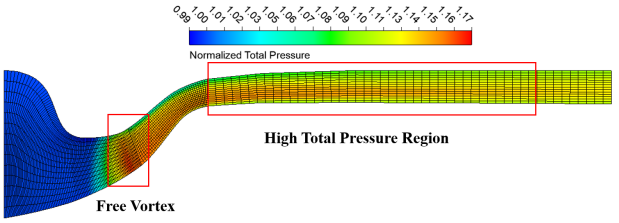

(c) Free vortex stage

FIGURE 13: Mass averaged total pressure contours in meridional plane

Stator Design

Downstream of the impeller, a stator is designed to guide the flow, which consists of 13 blades. Fig. 14 shows the normalized total pressure contours on the meridional plane of the whole stage. The flow path geometry of the stator has a fairly uniform area before its turning to axial to avoid flow separation. The stator flow path diverging occurs after it turns to axial with an area ratio of outlet to inlet of 1.05, which achieves an excellent high stator total pressure recovery of 99.29%. Besides, the stator blades decrease the swirl angle and its variation in span, which reduce the downstream mixing loss. Fig. 15 shows the swirl angle and Mach number distribution of stator inlet and outlet. The averaged flow velocity across the stator is decreased by 13% and the averaged swirl angle is decreased by 11°.

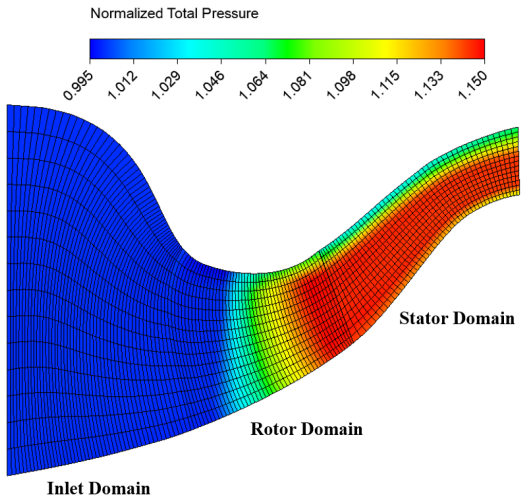

FIGURE 14: Normalized total pressure contours of single stage

Copyright © 2019 by ASME

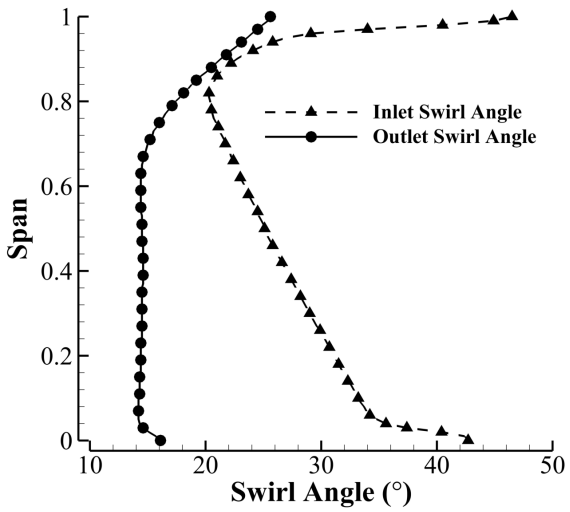

(a) Stator swirl angle distribution

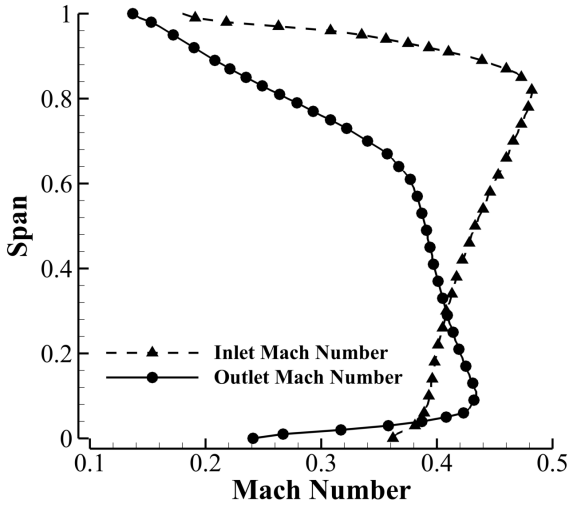

(b) Stator Mach number distribution

FIGURE 15: Parameters spanwise distribution across stator

The computed stage performance is calculated using single passage computational domain and is plotted in Fig. 16 that includes three speedlines ranging from 75000 to 120000. The stage is designed at 93000 with a total pressure ratio of 1.117 and a efficiency of 84.3% at the design point. A large stall margin (SM) [32] of 40.4% is achieved, based on Eq. 4. The design RPM of the compressor corresponds to the cruise condition of the CFJ aircraft, at which a high volume flow rate with a low pressure rise is needed for the CFJ micro-compressor actuators. The maximum RPM (120000) in Fig. 16 represents the take-off condition, at which the maximum power is required to generate a transient high lift coefficient for CFJ wing. A total pressure ratio of 1.3 is achieved by the micro-compressor operating at the maximum RPM.

$$SM = 1 - \left[\frac{(p_{02}/p_{01})_{design}}{(p_{02}/p_{01})_{stall}} \times \frac{m_{cor-stall}}{m_{cor-design}} \right] \tag{4}$$

where m_{cor} is the corrected mass flow rate defined by $\dot{m}\frac{\sqrt{T_0}}{p_0}$.

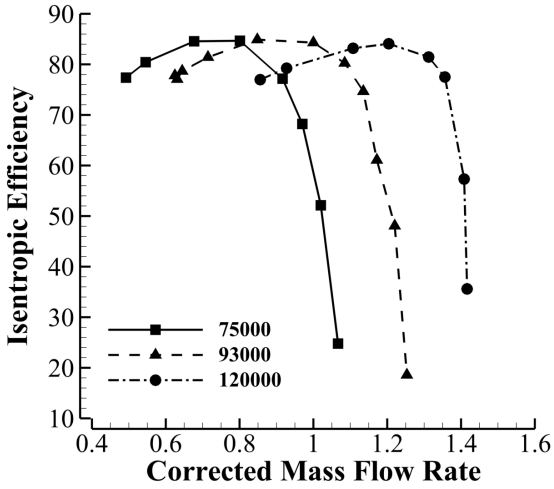

(a) Isentropic efficiency

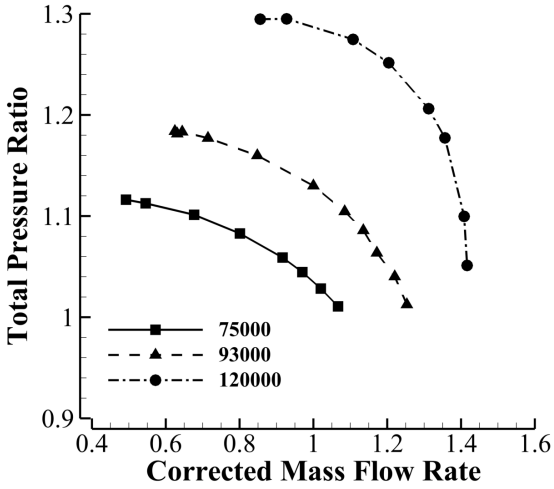

(b) Total pressure ratio

FIGURE 16: Stage performance at different RPM

Copyright © 2019 by ASME

OGV and Nozzle Design

Downstream the micro-compressor stage, an OGV is required to deswirl the flow to less than 10 ° and decrease the static pressure to match the CFJ airfoil leading edge low pressure of suction peak. A ratio of the actuator outlet static pressure to the compressor inlet total pressure of 0.987 is required by the OGV and the nozzle.

The OGV with a straight outlet duct is used as the preliminary design. The mass averaged total pressure contours on the meridional plane is presented in Fig. 17 (a). It is observed that the total pressure is dissipated quickly as flow approaches downstream. More efforts will be made to reduce the loss of the OGV and nozzle. Design optimization to improve the total pressure recovery for the OGV and outlet duct is in progress and will be reported in [33].

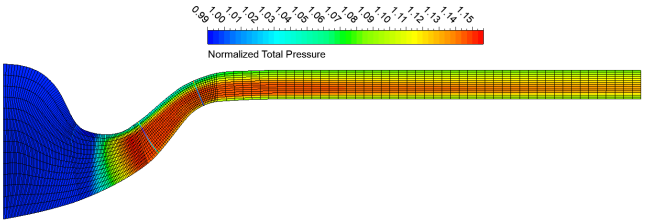

FIGURE 17: OGV and nozzle in straight channel

Mechanical Design

The preliminary structure analysis of impeller blade including Mises stress and modal analysis were performed using ABAQUS. The Finite Element Model (FEM) is a single impeller blade, meshed with H-mesh, shown in Fig. 18. The material properties are based on aluminum alloy.

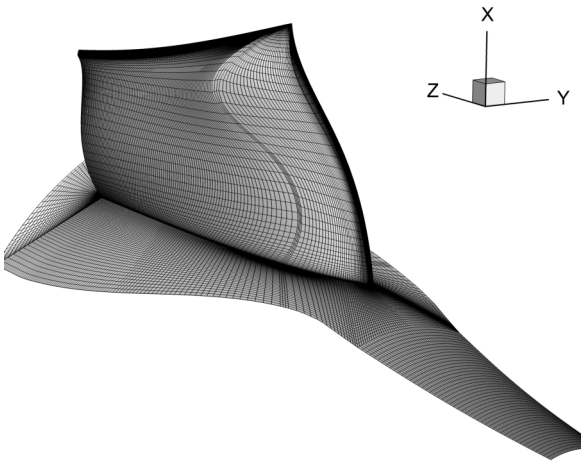

FIGURE 18: Computational domain of structure analysis

To ensure the structure strength of impeller blade, the centrifugal load was applied with maximum operating speed (12566 rad/sec), which produces a maximum Mises stress of 250 Mpa located at the blade hub as shown in Fig. 19. The maximum yield strength of the material is 440 MPa. Therefore the impeller has a safety factor of 1.76.

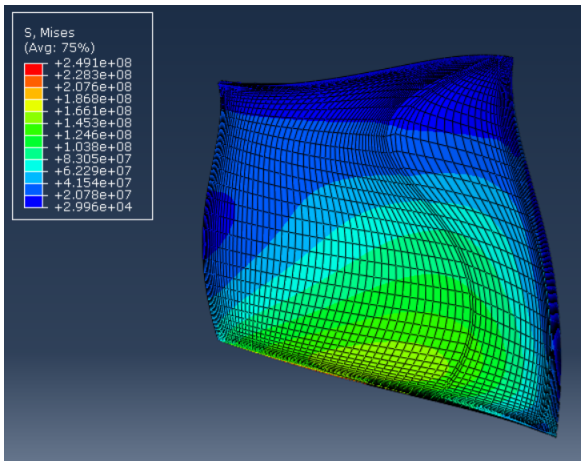

FIGURE 19: Contour of mises stress of impeller blade

It is pointed out by Casey that "the fundamental mode frequency should exceed that of the 4th engine order at the maximum normal operating speed" [6]. The present impeller also satisfies this criterion.

CONCLUSIONS

A high specific speed mixed flow micro-compressor used as the actuator for Active Flow Control airfoil is designed in this paper. The numerical design approach is validated with a mixed micro-compressor with very good agreement between the predicted performance and the measured data. Front loaded rotor blade work distribution is adopted to decrease boundary layer loss at the blade surface. Free vortex work distribution is applied for the rotor span to reduce spanwise mixing loss. The predicted rotor efficiency is 91.7%. Significant loss is observed downstream of the rotor when the flow enters the stator and outlet guide vane (OGV). For the stator, it is found that an inlet and outlet area ratio of 1.05 achieves an excellent high total pressure recovery of 99.29%. A very good stage isentropic efficiency of 84.3% is achieved. The final design of the micro-compressor achieves a flow coefficient of 0.3 at the design point with a total pressure ratio of 1.117 and a static pressure ratio of 0.987. A structure FEM analysis indicates that the rotor blades satisfy the structure strength and modal frequency requirement.

Copyright © 2019 by ASME

The present work indicates that a high power density, high mass flow rate and high efficiency design of micro-compressor for flow control is achievable. More work to optimize the OGV and outlet nozzle is in progress as a separated design effort to minimize the total pressure loss and match the low static pressure requirement at different operating conditions of CFJ airfoil.

ACKNOWLEDGMENT

We thank the fruitful discussion with Christof Zwyssig and his colleagues at Celeroton for the design constraints to make the micro-compressor aerodynamic design feasible for manufacturing.

REFERENCES

[1] Musgrave, D., and Plehn, N., 1987. "Mixed-flow compressor stage design and test results with a pressure ratio of 3: 1". *Journal of turbomachinery,* ***109***(4), pp. 513–519.

[2] Mönig, R., Broichhausen, K., and Gallus, H., 1987. Application of highly loaded single-stage mixed flow compressors in small jet-engines. Tech. rep., MOTOREN-UND TURBINEN-UNION GMBH MUNICH (GERMANY FR).

[3] Mönig, R., Elmendorf, W., and Gallus, H., 1992. "Design and rotor performance of a 5: 1 mixed-flow supersonic compressor". In ASME 1992 International Gas Turbine and Aeroengine Congress and Exposition, American Society of Mechanical Engineers, pp. V001T01A040–V001T01A040.

[4] Rodgers, C., 1996. "Development of a high specific speed centrifugal compressor". In ASME 1996 International Gas Turbine and Aeroengine Congress and Exhibition, American Society of Mechanical Engineers, pp. V001T01A087–V001T01A087.

[5] Casey, M., Zwyssig, C., and Robinson, C., 2010. "The cordier line for mixed flow compressors". In ASME Turbo Expo 2010: Power for Land, Sea, and Air, American Society of Mechanical Engineers, pp. 1859–1869.

[6] Hazby, H., Casey, M., Numakura, R., and Tamaki, H., 2015. "A transonic mixed flow compressor for an extreme duty". *Journal of Turbomachinery,* ***137***(5), p. 051010.

[7] Casey, M., and Robinson, C., 2011. "A unified correction method for reynolds number, size, and roughness effects on the performance of compressors". *Proceedings of the Institution of Mechanical Engineers, Part A: Journal of Power and Energy,* ***225***(7), pp. 864–876.

[8] Dietmann, F., and Casey, M., 2013. "The effects of reynolds number and roughness on compressor performance". In Proceedings of the 10th European Conference on Turbomachinery: Fluid Dynamics and Thermodynamics, Lappeenranta, Finland, pp. 15–19.

[9] Heß, M., and Pelz, P. F., 2010. "On reliable performance prediction of axial turbomachines". In ASME Turbo Expo 2010: Power for Land, Sea, and Air, American Society of Mechanical Engineers, pp. 139–149.

[10] Tiainen, J., Jaatinen-Värri, A., Grönman, A., and Backman, J., 2016. "Numerical study of the reynolds number effect on the centrifugal compressor performance and losses". In ASME Turbo Expo 2016: Turbomachinery Technical Conference and Exposition, American Society of Mechanical Engineers, pp. V02DT42A002–V02DT42A002.

[11] Zha, G.-C., F Carroll, B., Paxton, C. D., Conley, C. A., and Wells, A., 2007. "High-performance airfoil using coflow jet flow control". *AIAA journal,* ***45***(8), pp. 2087–2090.

[12] Lefebvre, A., Dano, B., Bartow, W., Fronzo, M., and Zha, G., 2016. "Performance and energy expenditure of coflow jet airfoil with variation of mach number". *Journal of Aircraft,* ***53***(6), pp. 1757–1767.

[13] G. Zha, W. Gao, and C.D. Paxton, 2007. "Jet Effects on Co-Flow Jet Airfoil Performance". *AIAA Journal,* ***45***, pp. 1222–1231.

[14] G.-C. Zha, C. Paxton, A. Conley, A. Wells, nd B. Carroll, 2006. "Effect of Injection Slot Size on High Performance Co-Flow Jet Airfoil". *AIAA Journal of Aircraft,* ***43***, pp. 987–995.

[15] Yang, Yunchao and Zha, Gecheng, 9-13 January 2017. "Super-Lift Coefficient of Active Flow Control Airfoil: What is the Limit?". *AIAA Paper 2017-1693, AIAA SCITECH2017, 55th AIAA Aerospace Science Meeting, Grapevine, Texas*, p. 1693.

[16] Dano, B. P. E., Kirk, D., and Zha, G.-C., 28 Jun - 1 Jul 2010. Experimental Investigation of Jet Mixing Mechanism of Co- Flow Jet Airfoil. AIAA-2010-4421, 5th AIAA Flow Control Conference, Chicago, IL.

[17] Dano, B., Zha, G., and Castillo, M., 2011. Experimental study of co-flow jet airfoil performance enhancement using discreet jets.

[18] Lefebvre, A. and Zha, G.-C. , 5-9 Jan 2015. Design of High Wing Loading Compact Electric Airplane Utilizing Co-Flow Jet Flow Control. AIAA Paper 2015-0772, AIAA SciTech2015: 53nd Aerospace Sciences Meeting, Kissimmee, FL.

[19] Lefebvre, A. and Dano, B. and Bartow, W. and Di Franzo, M. and Zha, G.-C., 2016. Performance Enhancement and Energy Expenditure of Co-Flow Jet Airfoil with Variation of Mach Number. AIAA Paper 2013-0490, AIAA Journal of Aircraft, DOI: 10.2514/1.C033113.

[20] Liu, Z.-X. and Zha, G.-C., June 13-17 2016. Transonic Airfoil Performance Enhancement Using Co-Flow Jet Active Flow Control. AIAA Paper 2016-3066, AIAA Aviation.

[21] Lefebvre, A. and Zha, G.-C., 4-8 January 2016. Trade Study of 3D Co-Flow Jet Wing for Cruise Performance. AIAA Paper 2016-0570, AIAA SCITECH2016, AIAA

Copyright © 2019 by ASME

Aerospace Science Meeting, San Diego, CA.
[22] Jinhuan, Z., Kewei, X., Yang, Y., Ren Yan, P. P., and Zha, G., 2018. "Aircraft control surfaces using co-flow jet active flow control airfoil". *AIAA Aviation and Aeronautics Forum and Exposition 2018*.
[23] Kewei, X., Jinhuan, Z., and Zha, G., 2019. "Drag minimization of co-flow jet control surfaces at cruise conditions". *AIAA Science and Technology Forum 2019*.
[24] Zha, G., Yang, Y., Ren, Y., and McBreen, B., 2018. "Superlift and thrusting airfoil of coflow jet actuated by micro-compressors". In 2018 Flow Control Conference, p. 3061.
[25] Hazby, H., Casey, M., Numakura, R., and Tamaki, H., 2014. "Design and testing of a high flow coefficient mixed flow impeller". In 11th International Conference on Turbochargers and Turbocharging: 13-14 May 2014: 13-14 May 2014, Vol. 1384, Elsevier, p. 55.
[26] Balje, O., 1981. *Turbomachines-A guide to design, selection, and theory*. No. BOOK. John Wiley & Sons.
[27] Cordier, O., 1953. "Ähnlichkeitsbedingungen für strömungsmaschinen". *BWK Bd,* ***6***.
[28] Robison, C., Feb. 23, 2017. "Design of a mixed flow fan". Vol. PCA-211-3-rep1-1, PCA Engineering Limited.
[29] Zwyssig, C., Oct. 24, 2017.. "Design of a mixed flow fan prototype". Vol. PR-4241-011, Celereton.
[30] Patel, P., and Zha, G., 2019. "Investigation of mixed micro-compressor casing treatment using non-matching mesh interface". In ASME Turbo Expo 2019 Turbomachinery Technical Conference and Exposition, American Society of Mechanical Engineers.
[31] Coppage, J., and Dallenbach, F., 1956. Study of supersonic radial compressors for refrigeration and pressurization systems. Tech. rep., GARRETT CORP LOS ANGELES CA AIRESEARCH MFG DIV.
[32] Cumpsty, N. A., 1989. *Compressor aerodynamics*. Longman Scientific & Technical.
[33] Kewei, X., and Zha, G., 2019. "Improving efficiency of co-flow jet micro-compressor actuator outlet guide vanes and nozzle". *AIAA AIAA Science and Technology Forum 2019*.

Copyright © 2019 by ASME